Journal of Visualized Experiments

Quantification of Biventricular Function and Morphology by Cardiac Magnetic Resonance Imaging in Mice with Pulmonary Artery Banding

--Manuscript Draft--

Article Type:	Invited Methods Article - JoVE Produced Video
Manuscript Number:	JoVE60837R2
Full Title:	Quantification of Biventricular Function and Morphology by Cardiac Magnetic Resonance Imaging in Mice with Pulmonary Artery Banding
Section/Category:	JoVE Medicine
Keywords:	right ventricular pressure load, mice model, pulmonary artery banding, cardiac magnetic resonance, ventricular dimensions, cardiac remodeling, hypertrophy, dilatation, cardiac function
Corresponding Author:	Anne-Marie Koop, MD Universitair Medisch Centrum Groningen Universitair Centrum Psychiatrie GRONINGEN, GRONINGEN NETHERLANDS
Corresponding Author's Institution:	Universitair Medisch Centrum Groningen Universitair Centrum Psychiatrie
Corresponding Author E-Mail:	a.c.koop@umcg.nl
Order of Authors:	Anne-Marie C. Koop
	Quint A.J. Hagdorn
	Kees W.A. van de Kolk
	Annemieke van Oosten
	Michel Weij
	Herman H.W. Silljé
	Tineke P. Willems
	Rolf M.F. Berger
Additional Information:	
Question	**Response**
Please indicate whether this article will be Standard Access or Open Access.	Standard Access (US$2,400)
Please indicate the **city, state/province, and country** where this article will be **filmed**. Please do not use abbreviations.	Groningen, The Netherlands

TITLE:

Quantification of Biventricular Function and Morphology by Cardiac Magnetic Resonance Imaging in Mice with Pulmonary Artery Banding

AUTHORS AND AFFILIATIONS:

Anne-Marie C. Koop[1]*, Quint A. J. Hagdorn[1]*, Kees (C.) W. A. van de Kolk[2,3], Annemieke van Oosten[2], Michel Weij[2], Herman H. W. Silljé[4], Tineke P. Willems[5], Rolf M. F. Berger[1]

[1]Center for Congenital Heart Diseases, Department of Pediatric Cardiology, University Medical Center Groningen, University of Groningen, Groningen, The Netherlands
[2] The Central Animal Facility, University Medical Center Groningen, University of Groningen, Groningen, The Netherlands
[3]Gronsai (Groningen Small Animal Imaging Facility), University Medical Center Groningen, University of Groningen, Groningen, The Netherlands
[4]Department of Cardiology, University Medical Center Groningen, University of Groningen, Groningen, The Netherlands
[5]Department of Radiology, University Medical Center Groningen, University of Groningen, Groningen, The Netherlands

* These authors contributed equally to the manuscript.

Corresponding Author:

Anne-Marie C. Koop (a.c.koop@umcg.nl)

Contributing Authors:

Quint A. J. Hagdorn (q.a.j.hagdorn@umcg.nl)
Kees (C.) W. A. van de Kolk (c.w.a.van.de.kolk@umcg.nl)
Annemieke van Oosten (a.van.oosten@umcg.nl)
Michel Weij (m.weij01@umcg.nl)
Herman H. W. Silljé (h.h.w.sillje@umcg.nl)
Tineke P. Willems (t.p.willems@umcg.nl)
Rolf M. F. Berger (r.m.f.berger@umcg.nl)

KEYWORDS:

right ventricular pressure load, mice model, pulmonary artery banding, cardiac magnetic resonance, ventricular dimensions, cardiac remodeling, hypertrophy, dilatation, cardiac function

SUMMARY:

To understand the pathophysiology of right ventricular (RV) adaptation to abnormal loading, experimental models are crucial. However, assessment of RV dimensions and function is complex and challenging. This protocol provides a method to perform cardiac magnetic resonance imaging (CMR) as a noninvasive benchmark procedure in mice subjected to RV pressure load.

ABSTRACT:

Right ventricular (RV) function and failure are major determinants of outcome in acquired and congenital heart diseases, including pulmonary hypertension. Assessment of RV function and morphology is complex, partly due to the complex shape of the RV. Currently, cardiac magnetic resonance (CMR) imaging is the golden standard for noninvasive assessment of RV function and morphology. The current protocol describes CMR imaging in a mouse model of RV pressure load induced by pulmonary artery banding (PAB). PAB is performed by placing a 6-0 suture around the pulmonary artery over a 23 G needle. The PAB gradient is determined using echocardiography at 2 and 6 weeks. At 6 weeks, the right and left ventricular morphology and function is assessed by measuring both end-systolic and end-diastolic volumes and mass by ten to eleven cine slices 1 mm thick using a 9.4 T magnetic resonance imaging scanner equipped with a 1,500 mT/m gradient. Representative results show that PAB induces a significant increase in RV pressure load, with significant effects on biventricular morphology and RV function. It is also shown that at 6 weeks of RV pressure load, cardiac output is maintained. Presented here is a reproducible protocol for the quantification of biventricular morphology and function in a mouse model of RV pressure load and may serve as a method for experiments exploring determinants of RV remodeling and dysfunction.

INTRODUCTION:

Patients with acquired and congenital cardiovascular diseases, including pulmonary hypertension (PH), are at risk of right ventricular (RV) dysfunction and failure[1]. RV adaptation as a result of increased pressure load is characterized by concentric hypertrophy in early stages and progressive dilatation in end-stage disease. Furthermore, it is associated with disorders in metabolism and the extracellular matrix, processes of inflammation and, eventually, RV failure[2–6]. Animal models have been developed to explore the underlying processes of the progression towards RV failure. However, optimization of models and adequate assessment of RV function and dimensions has been challenging. For noninvasive assessment of RV function and dimensions, cardiac magnetic resonance (CMR) imaging is the golden standard. This technique creates images of the beating heart by using a strong magnetic field and radiofrequency waves. CMR is available for humans, and for animals such as laboratory rodents. As the latter require higher spatial resolution due to the smaller size of the heart, the magnetic field required to provide adequate images must be higher, compared to humans.

Multiple models mimicking RV pressure overload are available, including models of PH[7–17] and models of proximal RV pressure load[2,3,10,18–23]. The choice of either a model of PH or a model of proximal RV pressure load depends on the research question: the effect of an intervention on the pulmonary vasculature and therefore possibly RV afterload modulation (i.e., PH models), or the direct effect on the RV (i.e., proximal RV pressure load models). Several methods for experimental induction of PH are available, including use of monocrotaline (MCT)[12–14,16,22,24–26], MCT combined with an aortocaval shunt[9], chronic hypoxia[7,27–29], and the combination of a vascular endothelial growth factor receptor antagonist, Sugen 5416, with chronic hypoxia[8,10,30,31]. Such models represent progressive pulmonary models of proximal RV pressure load and are not targeted at the pulmonary vasculature but induce a constant afterload by constriction of the pulmonary artery, with an accompanying increase of RV afterload[2,3]. This can be performed by a suture-banding (pulmonary artery banding, PAB) or a vascular clip around the pulmonary artery.

PAB has been performed in several animal species, and cardiac dimensions and function have been studied in various ways, such as histology, transthoracic echocardiography (including speckle tracking), and heart catheterization[2,32–40]. PAB in small rodents, such as mice, is challenging. This is because subtle differences between the tightness of artery constriction have marked results on the degree of RV pressure load and subsequent functional status and survival. When the constriction is very tight, the animal will die during or shortly after operation, whereas the desired phenotype will not be achieved when the constriction is not tight enough. However, the use of mice has advantages compared to other animals, because of the excellent genetic modification possibilities (i.e., transgenic or knockout models) and fast breeding. This is of added value in the study of diseases and in exploring the contribution of molecular and (epi-) genetic factors.

Animal study designs are shifting towards the investigation of temporal changes during disease[2,3,8,13,21]. For such studies, noninvasive modalities are necessary, because serial assessments can be performed. Alternatives to CMR in the assessment of cardiac remodeling could be (1) tissue characterization using histopathology, with multiple animals being sacrificed at different time points, (2) invasive functional assessment by pressure-volume analysis, or (3) echocardiography, which allows the researcher to identify cardiac hypertrophy or dilatation noninvasively within the same animal serially. CMR has two major advantages in assessment of the RV: (1) CMR is a noninvasive modality, enabling serial measurements in one animal, hereby contributing to reducing animal numbers needed for studies, and (2) CMR does not rely on a particular geometric shape and visualizes three-dimensionally. CMR-derived RV volumes and function measurements have been shown to be accurate and are considered to be the noninvasive golden standard in different cardiac entities in humans[42–45], but had not yet been translated to a CMR protocol for mice with RV pressure overload.

Many models of PAB are described in the literature, but with high heterogeneity in methods of assessing hemodynamic effects and RV function and adaptation. This protocol outlines the procedure of PAB in mice with validation of the model by measuring the PAB gradient by echocardiography and evaluating cardiac dimensions and function with CMR. While a protocol of CMR in animals subjected to PAB has been published for rats, this combination has not been described for mice until now. While rats are most commonly used for PH models[8,12–16,22,24–31,46], mice are most often used for transgenic or knock-out studies and thereby contribute to our understanding of mechanisms in pressure-loaded RV failure. This protocol could form the basis for future studies to unravel signaling pathways involved in the transition towards RV failure.

PROTOCOL:

All experiments and animal care are conducted according to the Dutch Animal Experimental Act and conform to the Guide for the Care and Use of Laboratory Animals published by the US National Institutes of Health. The Animal Experiments Committee of the University of Groningen, the Netherlands, approved the current experimental protocol (permit number: 2014-041/3005).

1. Housing and acclimatization

1.1.1. Use 20–30 g wild type C57 black 6 (C57BL/6) mice (institutional breeding line described previously[47]), male and female, all more than 8 weeks old. House the mice in groups with a maximum of five per cage. In order to get used to human handling, let the mice acclimatize for at least 7 days. Do not perform any procedures during this period.

2. Pulmonary artery banding surgery

2.1. Preparation

2.1.1. Place the mouse in the induction chamber filled with 5% isoflurane/100% oxygen. Check for the lack of reflexes by giving a pain stimulus (i.e., toe pinch).

2.1.2. Shave the left hemithorax of the mouse using an electric shaver.

2.1.3. Gently pull out the tongue and hold with mild tension.

2.1.4. Illuminate the inner throat by placing a light source on the exterior throat at the level of the glottis.

2.1.5. Intubate the mouse endotracheally with a 20 G flexible cannula.

2.1.6. Place the animal on its right side on a heat mat (set temperature at 37 °C).

2.1.7. Connect the cannula to the miniventilator and start ventilation with 1.5%–2.5% isoflurane/oxygen (180 breaths/min, tidal 250 µL).

2.1.8. Inject 0.1 mg/kg buprenorphine subcutaneously for postoperative analgesia.

2.1.9. Prevent dehydration of the eye using eye ointment.

2.2. Pulmonary artery banding surgery by left lateral thoracotomy

2.2.1. Place the mouse on its right side by placing the right foreleg in a neutral position, the right hind leg extended, and the left foreleg bent back.

2.2.2. Disinfect the skin on the thorax with chloride-hexidine, swab 2x.

2.2.3. Use sterile instruments for surgery. Open the skin with small scissors (round handle, 12 mm blades) from the left armpit parallel to the second and third rib.

2.2.4. Identify the m. pectoralis superficialis (oblique, superficial muscle) and the m. pectoralis profundus (oblique, underlying muscle).

2.2.5. Using suture loops, pull the m. pectoralis superficialis towards the ventral side and the m. pectoralis profundus towards the dorsal side of the mouse.

2.2.6. Open the second intercostal space and spread the ribs by using adapted paper clips, allowing the left heart ear, left lung, and the pulmonary artery to become visible.

2.2.7. Separate the arteria pulmonalis from the aorta. Place a suture loop around the pulmonary artery with a blunt 25 G needle that contains a 6-0 suture and place a lose 2-1-1 ligature around the arteria pulmonalis.

2.2.8. Place a 23 G needle parallel to the arteria pulmonalis within the 6-0 suture and first fix the most proximal suture knot and then distal knot of the 2-1-1 suture. Remove the 23 G needle. Make sure the knot is adequate.

2.2.9. Close the thorax with two or three separate sutures with a monofilament polypropylene 5-0 suture. Release the m. pectoralis superficalis and m. pectoralis profundus.

2.2.10. Suture the skin with a pure polyglycolic acid 5-0 suture. Use a continuous suture technique to minimize scar formation in the tissue; scar tissue will influence the image quality of the echocardiography.

2.2.11. Turn off the isoflurane while continuing ventilation with oxygen during recovery from anesthesia until the mouse regains its own, spontaneous respiration as can be observed from movement of the abdomen.

2.2.12. Uncouple the endotracheal tube from the ventilator. Check for spontaneous respiration, extubate only when spontaneous respiratory action is visible. When spontaneous respiration is not seen, connect the tube to the ventilator again and return to step 2.2.12.

2.2.13. Observe the mouse until it regains consciousness.

2.3. Sham surgery

2.3.1. Perform the above procedure with the exception of the banding (steps 2.2.2–2.2.6).

2.4. Postsurgical period

2.4.1. House the mouse individually in an incubator (37 °C) for 24 h.

2.4.2. Observe the mouse daily during the first 3 postoperative days. In case of any signs of discomfort, inject 0.1 mg/kg buprenorphine subcutaneously 2x daily for postoperative analgesia.

3. Echocardiography

3.1. Preparation

3.1.1. Perform PAB gradient analysis by means of echocardiography 14 days after PAB surgery.

3.1.2. Start the echocardiography device. Choose the cardiac package and a 14.0 MHz transducer.

3.2. Anesthesia

3.2.1. Place the mouse in the induction chamber filled with a mixture of 5% isoflurane and 100% oxygen.

3.2.2. Shave the thorax of the mouse.

3.2.3. Place the mouse on its back on the heat mat (temperature 37 °C) and place the snout in the ventilation mask.

3.2.4. Ventilate with a mixture of 1.5%–2.5% isoflurane and 100% oxygen (0.15 L/min) and room air (0.3 L/min).

3.2.5. Check the depth of the anesthesia by performing a toe pinch and adjust the anesthesia accordingly.

3.2.6. Prevent dehydration of the eye by using eye ointment.

3.3. Determination of PAB gradient by echocardiography

3.3.1. Place pediatric electrocardiogram-stickers on each foreleg and one on both hind legs. Use the stickers to hold the animal.

3.3.2. Apply ultrasound gel to the shaved part of the mouse's thorax.

3.3.3. To obtain the images of the pulmonary artery, two views can be used: the parasternal long axis (PLAX) or the parasternal short axis (PSAX) view. Obtain both and use the view that gives the best quality measurements and highest velocities for analysis.

3.3.4. Obtain PLAX and PSAX views.

3.3.5. Press the **color-Doppler button** to visualize blood flow.

3.3.6. Place the ultrasound probe at a 30° angle to the parasternal line to obtain PLAX (for detailed description see Cheng, et al.[48]), visualizing the ascending aorta.

3.3.7. Sweep the probe minimally towards the left so the ascending aorta disappears behind the pulmonary artery. The appropriate PLAX is identified when the pulmonary artery is visualized,

with blood flowing vertically.

3.3.8. Place the cursor in line with the pulmonary artery. Press the **continuous wave** (CW) **Doppler button** to derive velocity time integral measurements during three cardiac cycles. Press **Save**.

3.3.9. Rotate the probe 90° clockwise from the PLAX to obtain PSAX, then tilt the probe slightly towards the cranial/ventral direction to derive the PSAX at the aortic level. The appropriate PSAX view is identified if the RV outflow tract is situated between the aorta and the probe. This continues in the pulmonary artery, with blood flowing vertically. For a detailed description see Cheng et al.[48]

3.3.10. Place the cursor in line with the pulmonary artery. Press the **continuous wave** (CW) **Doppler button** to derive velocity time integral measurements during three cardiac cycles. Press **Save**.

3.3.11. Measure the three maximum velocities of the best view (PSAX or PLAX) and calculate the mean. Use the simplified Bernoulli's principle $delta - P = 4 \cdot V^2$ to derive the PAB gradient in millimeters mercury (mmHg).

4. Cardiac magnetic resonance imaging

4.1. Preparation

4.1.1. Perform CMR analysis 6 weeks (i.e., 42 days) after PAB surgery.

NOTE: Additionally, earlier timepoints after PAB surgery may be chosen when multiple timepoints are to be included, depending on the research question. Later timepoints could be considered; however, RV failure and death may increasingly occur.

4.1.2. Use a sufficiently powerful magnet (typically, >7 T is used for rodent CMR scanning). For the current protocol, a 9.4 T vertical system, with 1,500 mT/m gradient set and 89 mm bore size is used.

4.1.3. Install CMR postprocessing software for analyzing volumes and masses in the derived images. The software is deemed appropriate if it allows manual segmentation to determine end-diastolic (ED) and end-systolic (ES) volumes (EDV and ESV, respectively) and ventricular mass (measured both ED and ES).

4.2. Anesthesia and fixation

4.2.1. Place the mouse in the induction chamber filled with a mixture of 5% isoflurane and 100% oxygen. Verify the effect of the anesthesia by giving a pain stimulus by a toe pinch.

4.2.2. Put eye ointment on the eyes of the mouse to keep them moist during scanning.

4.2.3. Place the mouse in the scanner's animal bed with integrated air supply, a warmed (37 °C) mixture of 1.5%–2.5% isoflurane, 100% oxygen (0.15 L/min), and room air (0.3 L/min), and a pressure pad that enables observation of heart rate (aim for 400–500 bpm) and respiratory rate (aim for ~35 breaths per min) during scanning. Regulate the anesthesia based those two parameters. Make sure the bed is made of plastic, without any magnetic material.

4.2.4. Place the animal bed with the mouse into the scanner.

4.3. Performing cardiac magnetic resonance imaging

4.3.1. Make preacquisition adjustments by tuning the radiofrequency (RF) birdcage coil on 1 Hydrogen (1 H) resonance frequency.

4.3.2. Then set the magnetic field as homogeneous as possible using the automatic shimming procedure.

NOTE: The computerized shimming is done by the so-called Tuning method, which uses the area under the 1 H FID as a quality parameter. In this Tuning procedure a user-defined group of shims (Z, Z2, X, Y, XZ, and YZ) is examined in an iterative cycle. Each shim in succession is adjusted individually to maximize the area under the FID. This is essentially a linear procedure that works well quickly.

4.3.3. Optimize the RF pulse by maximizing the one-dimensional image profile with adjustment of RF pulse power.

4.3.4. Assign the exact position of the heart in the scanner by making scout scans using a tripilot sequence. Use a fast gradient echo sequence to acquire the scout images through the thorax: a transversal, coronal, and sagittal slice. (**Figure 1A**,**B**,**C**)

4.3.5. Adjust the axes to the actual axes of the axial, two-chamber, and four-chamber view (**Figure 1D**,**E**).

4.3.6. Subsequently, position the cine slices perpendicular to an imaginary axis between the RV outflow tract and the utmost apical part of the RV.

4.3.7. Derive ten to eleven 1 mm-thick cine slices without a slice gap to cover the entire top to base imaging of the RV (**Figure 1F**) by means of the Self-gated IntraGate-fast low-angle shot (FLASH) method, which obviates the need for an electrocardiogram (ECG) and respiratory gating. The acquisition parameters are displayed in **Table 1**. Save the images in DICOM format.

4.4. Performing analyses on acquired images

4.4.1. Double click on the software to open the program.

4.4.2. Open images in the CMR postprocessing software by using the **import** button.

4.4.3. Identify the end-systolic phase (defined as the phase with the visually smallest RV cavity) and the end-diastolic phase (defined as the phase with the visually largest RV cavity).

4.4.4. According to guidelines from the Society for Cardiovascular Magnetic Resonance[49], draw the epicardial contours manually in end-diastole and end-systole from apex to base, by marking several points at the epicardial border of each image. At the last point, double click to complete the epicardial contour.

4.4.5. Do the same for the endocardial contours. (**Figure 2**). The left ventricular and right ventricular EDV, ESV, ED mass, and ES mass are now automatically calculated by the software.

NOTE: Mass is defined as myocardial volume times myocardial density (i.e., 1.05).

4.4.6. Depending on the research question and population under study, index these variables for subject size by means of tibia length or body weight, according to previously published formulas[50].

4.4.7. Calculate the eccentricity index (EI) both in end-diastole and end-systole, by dividing the diameter of the LV cavity parallel to the intraventricular septum (IVS) by the diameter of the LV cavity perpendicular to the IVS, derived from the short axis at midpapillary level.

4.4.8. The software calculates the stroke volume (SV) in mL as $SV = EDV - ESV$, and ejection fraction (EF, %) as $\mathrm{EF} = 100 * \frac{EDV-ESV}{EDV}$.

4.4.9. Calculate the cardiac output (CO) in ml/min as $\mathrm{CO} = \mathrm{SV} \cdot \mathrm{heart\ rate}$. The heart rate is measured manually by the pressure pad embedded in the animal bed as described above, because the scanner is not able to register the high frequent heart rate adequately.

4.4.10. Depending on the research question and population under study, index the CO and SV for subject size by means of tibia length or body weight, according to previously published formulas[50].

5. Statistical analyses

5.1. Open the software used for data visualization and statistical analyses.

5.2. Sort the data per group (PAB and sham) with every group in a separate column.

5.3. Use the Mann-Whitney test to compare PAB versus sham for every variable.

REPRESENTATIVE RESULTS:

Mortality rate of the PAB surgical procedure is around 10%. The presented results show characteristics of mice in the sham (n = 5) and PAB (n = 8) groups. As shown in **Figure 3**, PAB gradient values significantly increased compared to sham animals at 2 and 6 weeks after PAB. This increase of loading caused RV dilatation expressed as increased RV, EDV, and RV ESV (**Figure 4A**,**B**). RV dysfunction occurred as RV EF decreased (**Figure 4C**). RV SV remained unaffected (**Figure 4D**). RV ED and RV ES mass increased, indicating right ventricular hypertrophy (**Figure 4E**,**F**). LV EDV and LV ESV decreased (**Figure 4G**,**H**). LV function in terms of LV EF and LV SV was unaffected (**Figure 4I**,**J**). Neither LV ED or LV ES mass changed (**Figure 4K**,**L**). Septal flattening at both end-diastole and end-systole occurred, reflected by significant decreases of both eccentricity indexes (**Figure 4M**,**N**). Heart rate and SV were not different between PAB and sham animals and thus CO was unaffected (**Figure 4P**,**Q**). **Figure 4O** shows representative CMR images at midpapillary level, in end-diastole (top) and end-systole (below) in sham (left) and PAB (right).

FIGURE AND TABLE LEGENDS:

Figure 1: Slice orientation and planning. (**A**) Axial scout image, (**B**) coronal scout image, and (**C**) sagittal scout image. (**D**) Adjustment of the orientation slice for a two-chamber view (2CV) image. (**E**) Adjustment of the orientation slice for a four-chamber view (4CV) image. (**F**) Slice planning for cardiac cine imaging.

Figure 2: CMR quantification. For quantification, the endocardial (red for LV, yellow for RV) and epicardial (green for LV, blue for RV) contours were delineated in end-diastole (ED, top) and end-systole (ES, bottom) in a stack of short axis slices that covered both ventricles. These are shown in a sham and a pulmonary artery banding (PAB) mouse.

Figure 3: PAB gradient measured by Doppler echocardiography. Measurements were performed at 2 and 6 weeks respectively in the sham (n = 5) and pulmonary artery banding (PAB, n = 8) groups. The statistical analyses were performed using the Mann-Whitney test. Values are presented as median and interquartile range. * = $p < 0.05$ compared to sham. ○ = individual animal. PSAX = parasternal short axis. PLAX = parasternal long axis. LV = left ventricle.

Figure 4: Representative results of morphological and functional changes. The first panel shows RV parameters: RV EDV (**A**), RV ESV (**B**), RV EF (**C**), RV ED mass (**E**), and RV ES mass (**F**). The LV parameters are shown in the second panel: LV EDV (**G**), LV ESV (**H**), LV EF (**I**), LV SV (**J**), LV ED mass (**K**), and LV ES mass (**L**). Septal deviation is represented by the eccentricity index ED (**M**) and ES (**N**). Cardiac dimensions are shown in representative images (**O**). Heart rate (**P**) and cardiac output (**Q**) are also shown. The changes were observed due to 6 weeks of PAB measured by CMR in the sham (n = 5) and pulmonary artery banding (PAB, n = 8) groups. The statistical analyses were performed using the Mann-Whitney test. Values are presented as median and interquartile range. * = $p < 0.05$ compared to sham. ○ = individual animal. RV = right ventricle. LV = left ventricle. ED = end diastolic. ES = end systolic. EDV = ED volume. ESV = ES volume. SV = stroke volume. CO = cardiac output. EF = ejection fraction.

Table 1. Acquisition parameters of the CMR protocol.

DISCUSSION:

This protocol provides a reproducible method for PAB in mice and the subsequent assessment of cardiac remodeling and functional adaptation using CMR.

PAB differs from other models of increased RV pressure load because it involves absolute and static increase of afterload without the presence of other triggers. RV pressure load in models of hypoxia, monocrotaline, shunt, or a combination of these inducers are based on remodeling of the pulmonary vasculature. This remodeling is driven by endothelial damage, inflammation, cytokine migration, and vasoconstriction. The degree of these processes differs per model, therefore the degree of pressure load differs subsequently. In contrast to these models, PAB induces fixed RV afterload and is therefore reproducible and not affected by therapeutic interventions. This allows for the study of interventions targeting the pressure-loaded RV without affecting the RV afterload. This model of PAB in mice shows a significant gradient across the PAB and enables evaluation of this substantial pressure load.

Dimensional evaluation by echocardiography is challenging due to the triangular shape of the RV wrapped around the LV, and its position immediately behind the sternum[41,42]. Echocardiography, both 2D and 3D, has shown to be inferior compared to CMR[51,52]. In pediatric cohorts with congenital heart diseases, echocardiographic volumetry shows lower reliability and systematic underestimation compared to CMR[53,54]. Results regarding myocardial deformation measurements are still preliminary in this specific group of patients[55–57]. Of course, in clinical practice, echocardiography is a very accessible tool to identify abnormal loading conditions by recognition of shunts and valve insufficiencies in case of volume load, and stenosis and pulmonary hypertension by increased gradients and septal flattening in case of pressure load. Pressure-volume analysis by means of invasive heart catheterization is an available alternative for invasive hemodynamic and functional assessments. This technique is widely regarded indicative for load-independent ventricular function, but also comes with limitations that currently hamper the theoretical benchmark status of PV-loops in RV in small animals. For example, deriving reproducible and accurate volume and flow measurements is challenging in these small animals and many procedures require open-chest measurements. Furthermore, serial assessments are difficult if not unfeasible due to the invasive nature of the technique. Compared to both echocardiography and catheterization, assessment of volumes and function will be more accurate with CMR. In research, it is important for translatability to obtain results using modalities that can also be used for clinical practice. Therefore, development of standardized methods and optimization in experimental protocols is highly relevant.

The current protocol describes the use of self-gated CMR, which obviates the need for ECG triggering and respiratory gating. This method has been described previously in a report from the same institution, demonstrating good intra- and interobserver variability[58]. Another method that could be used if the self-gated method is unavailable, is prospective ECG triggering. However, a previous report from this institution demonstrated that the self-gated method provides less

variability, better signal and contrast-to-noise ratios, and less arrhythmia-induced artifacts. Therefore, we recommend using the self-gated method, as stated in the current protocol.

Accurate assessment of RV pressure load is crucial in order to validate the PAB model. This can be performed by means of invasive heart catheterization, for example. However, disadvantages of such invasive procedures are that they are very hazardous and complex to perform serially or during the follow-up time of the study and are therefore generally performed just before termination. However, at termination, RV pressure is not only dependent on the tightness of the banding but becomes increasingly dependent on RV function. Whenever RV failure occurs within the duration of PAB, as measured by decreased cardiac output, RV systolic pressure will decrease, biasing results. Such biases can be avoided or minimized by assessing RV pressure load at 2 weeks after PAB surgery, instead of at termination. By means of echocardiography, assessment of RV afterload at this time point can be performed reliably and safely. This allows grouping of the mice into groups with equal pressure load, which could be helpful for intervention studies. Also, repeated measurements are easily feasible.

The most critical step in the surgical protocol is the separation of the arteria pulmonalis from the aorta and the subsequent placement of the suture loop. This has to be performed gently in order not to cause any rupture, because this would result in fatal bleeding. PAB in mice requires that well-trained microsurgeons perform the actual banding, including knotting the suture, which should be done very carefully.

The current model aims to generate chronic RV pressure load, resulting in RV remodeling, RV dysfunction, and eventually RV failure. Therefore, adequate tightening of the PAB is important. During the development of the model, it has become apparent that small differences in tightness of the banding significantly affected the profile of RV adaptation: e.g., the use of a 25 G needle appeared to be “too tight”, as it induced high rates of mortality during surgery. Needles <23 G were “too loose”, as they did not induce the desired phenotype of RV remodeling and dysfunction.

The most critical step in the echocardiographic examination is adequate measurement of pulmonary flow velocity (step 3.3.7). One has to make sure that the angle of the probe is correct: the pulmonary artery has to be exactly vertically visible within the image. Otherwise, flow velocity, and therefore the PAB gradient, are underestimated.

It is important to try to limit the length of time of the procedures during the experiment, especially CMR. Furthermore, when analyzing the CMR images with postprocessing software, the researcher must become familiar with the manual segmentation and postprocessing guidelines before reproducible results can be obtained.

Using CMR as in the current protocol does not enable assessment of flow velocities over the PAB. Therefore, additional echocardiographic measurements using the Doppler mode are inevitable. Due to the PAB and the subsequent marked increase in PA flow, the signal is very clear, making determination of the PAB gradient by echocardiography convenient and reproducible.

Notwithstanding, the extra echocardiographic measurements may involve more logistical arrangements. In general, inclusion or exclusion of papillary muscles and trabeculae affects volumes and subsequent functional parameters. Here, we chose to include papillary muscles and trabeculae in blood volumes (and thus exclude from myocardial mass) which may underestimate the ejection fraction. Furthermore, the current protocol focuses on parameters used in clinical practice, representing global function. Parameters such as the tricuspid annular plane systolic excursion (TAPSE), fractional septum to free wall distance at the middle of the RV (fSFD), and fractional tricuspid annulus-apex distance change (fTAAD) were not analyzed.

A major advantage of CMR is the ability to perform noninvasive, serial testing within one subject with a relatively high accuracy of volumetric and functional measurements. Because it is a measurement after which the animal can survive, unlike open-chest pressure-volume analysis, for example, it allows for a follow-up after the measurements. Although we have focused on cardiac dimensions and function, future uses of this technique include CMR-derived tissue characterization or scar tissue assessment by means of late gadolinium enhancement. This enables reduction of histopathological assessments, which will lead to a reduction in animals required for studies. More CMR research may optimize tissue characterization in humans and reduce iatrogenic damage due to biopsies.

In conclusion, this protocol was created to provide guidance in the assessment of cardiac morphology and function in mice exposed to increased RV pressure load. The combination of PAB with CMR improves standardization and reproducibility. This makes it a very valuable technique for the study of signaling pathways involved in the failure of the pressure-loaded RV by the use of transgenic or knockout mice.

ACKNOWLEDGMENTS:

We would like to thank P. Da Costa-Martins for her support with the animal experiments in this study.

DISCLOSURES:

The University Medical Center Groningen has contracted with Actelion and Lilly for consultancy activities of R.M.F. Berger outside the content of this manuscript. The other authors declare that they have no competing interests.

REFERENCES:

1. Norozi, K. et al. Incidence and Risk Distribution of Heart Failure in Adolescents and Adults With Congenital Heart Disease After Cardiac Surgery. *The American Journal of Cardiology*. **97** (8), 1238–1243 (2006).
2. Borgdorff, M. A. J. et al. Clinical symptoms of right ventricular failure in experimental chronic pressure load are associated with progressive diastolic dysfunction. *Journal of Molecular and Cellular Cardiology*. **79**, 244–53 (2015).
3. Koop, A. M. C. et al. Right ventricular pressure overload alters cardiac lipid composition. *International Journal of Cardiology*. In press. (2019).
4. Faber, M. J. et al. Right and left ventricular function after chronic pulmonary artery

banding in rats assessed with biventricular pressure-volume loops. *American Journal of Physiology and Heart Circirculation Physiology*. **291** (4), H1580–H1586 (2006).
5. Bogaard, H. J. et al. Chronic pulmonary artery pressure elevation is insufficient to explain right heart failure. *Circulation*. **120** (20), 1951–1960 (2009).
6. Samson, N., Paulin, R. Epigenetics, inflammation and metabolism in right heart failure associated with pulmonary hypertension. *Pulmonary Circulation*. **7** (3), 572–587 (2017).
7. Rumsey, W. L. et al. Adaptation to hypoxia alters energy metabolism in rat heart. *American Journal of Physiology Heart and Circulatory Physiology*. **276** (1 45-1), H71–H80 (1999).
8. Drozd, K. et al. Effects of an endothelin receptor antagonist, Macitentan, on right ventricular substrate utilization and function in a Sugen 5416/hypoxia rat model of severe pulmonary arterial hypertension. *Journal of Nuclear Cardiology*. **24** (6), 1979–1989 (2017).
9. Van Der Feen, D. E. et al. Shunt surgery, right heart catheterization, and vascular morphometry in a rat model for flow-induced pulmonary arterial hypertension. *Journal of Visualized Experiments*. (120), e55065 (2017).
10. Gomez-Arroyo, J. et al. Metabolic gene remodeling and mitochondrial dysfunction in failing right ventricular hypertrophy secondary to pulmonary arterial hypertension. *Circulation: Heart Failure*. **6** (1), 136–144 (2013).
11. Bruns, D. R., Dale Brown, R., Stenmark, K. R., Buttrick, P. M., Walker, L. A. Mitochondrial integrity in a neonatal bovine model of right ventricular dysfunction. *American Journal of Physiology - Lung Cellular and Molecular Physiology*. **308** (2), L158–L167 (2015).
12. Zhang, W.-H. et al. Up-regulation of hexokinase1 in the right ventricle of monocrotaline induced pulmonary hypertension. *Respiratory Research*. **15** (1), 119 (2014).
13. Paulin, R. et al. A miR-208-Mef2 axis drives the decompensation of right ventricular function in pulmonary hypertension. *Circulation Research*. **116** (1), 56–69 (2015).
14. Sutendra, G. et al. A metabolic remodeling in right ventricular hypertrophy is associated with decreased angiogenesis and a transition from a compensated to a decompensated state in pulmonary hypertension. *Journal of Molecular Medicine*. **91** (11), 1315–1327 (2013).
15. Balestra, G. M. et al. Increased in vivo mitochondrial oxygenation with right ventricular failure induced by pulmonary arterial hypertension: Mitochondrial inhibition as driver of cardiac failure? *Respiratory Research*. **16**, 6 (2015).
16. Piao, L. et al. The inhibition of pyruvate dehydrogenase kinase improves impaired cardiac function and electrical remodeling in two models of right ventricular hypertrophy: Resuscitating the hibernating right ventricle. *Journal of Molecular Medicine*. **88** (1), 47–60 (2010).
17. Piao, L. et al. FOXO1-mediated upregulation of pyruvate dehydrogenase kinase-4 (PDK4) decreases glucose oxidation and impairs right ventricular function in pulmonary hypertension: therapeutic benefits of dichloroacetate. *Journal of Molecular Medicine*. **91**, 333–346 (2013).
18. Sheikh, A. M. et al. Right ventricular hypertrophy with early dysfunction: A proteomics study in a neonatal model. *Journal of Thoracic and Cardiovascular Surgery*. **137** (5), 1146–1153 (2009).
19. Olivetti, G. et al. Cellular basis of wall remodeling in long-term pressure overload-induced right ventricular hypertrophy in rats. *Circulation Research*. **63** (3), 648–657 (1988).
20. Lauva, I. K. et al. Control of myocardial tissue components and cardiocyte organelles in pressure-overload hypertrophy of the cat right ventricle. *The American Journal of Anatomy*. **177**

(1), 71–80 (1986).
21. Fang, Y.-H. et al. Therapeutic inhibition of fatty acid oxidation in right ventricular hypertrophy: Exploiting Randle's cycle. *Journal of Molecular Medicine*. **90** (1), 31–43 (2012).
22. Piao, L. et al. Cardiac glutaminolysis: A maladaptive cancer metabolism pathway in the right ventricle in pulmonary hypertension. *Journal of Molecular Medicine*. **91** (10), 1185–1197 (2013).
23. Sack, M. N., Disch, D. L., Rockman, H. A., Kelly, D. P. A role for Sp and nuclear receptor transcription factors in a cardiac hypertrophic growth program. *Proceedings of the National Academy of Sciences of the United States of America*. **94** (12), 6438–6443 (1997).
24. Broderick, T. L., King, T. M. Upregulation of GLUT-4 in right ventricle of rats with monocrotaline- induced pulmonary hypertension. *Medical Science Monitor*. **14** (12), BR261–BR264 (2008).
25. Enache, I. et al. Skeletal muscle mitochondrial dysfunction precedes right ventricular impairment in experimental pulmonary hypertension. *Molecular and Cellular Biochemistry*. **373** (1–2), 161–170 (2013).
26. Sun, X.-Q. et al. Reversal of right ventricular remodeling by dichloroacetate is related to inhibition of mitochondria-dependent apoptosis. *Hypertension Research*. **39** (5), 302–311 (2016).
27. Adrogue, J. V, Sharma, S., Ngumbela, K., Essop, M. F., Taegtmeyer, H. Acclimatization to chronic hypobaric hypoxia is associated with a differential transcriptional profile between the right and left ventricle. *Molecular and Cellular Biochemistry*. **278** (1–2), 71–78 (2005).
28. Sharma, S. et al. Dynamic changes of gene expression in hypoxia-induced right ventricular hypertrophy. *American Journal of Physiology - Heart and Circulatory Physiology*. **286** (3 55-3), H1185–H1192 (2004).
29. Nouette-Gaulain, K. et al. Time course of differential mitochondrial energy metabolism adaptation to chronic hypoxia in right and left ventricles. *Cardiovascular Research*. **66** (1), 132–140 (2005).
30. Graham, B. B. et al. Severe pulmonary hypertension is associated with altered right ventricle metabolic substrate uptake. *American Journal of Physiology - Lung Cellular and Molecular Physiology*. **309** (5), L435–L440 (2015).
31. Liu, A. et al. Estrogen maintains mitochondrial content and function in the right ventricle of rats with pulmonary hypertension. *Physiological Reports*. **5** (6), 1–12 (2017).
32. Kobr, J. et al. Right Ventricular Pressure Overload and Pathophysiology of Growing Porcine Biomodel. *Pediatric Cardiology*. **37** (8), 1498–1506 (2016).
33. Yerebakan, C. et al. Acute and chronic response of the right ventricle to surgically induced pressure and volume overload – an analysis of pressure–volume relations. *Interactive CardioVascular and Thoracic Surgery*. **10** (4), 519–525 (2010).
34. Gufler, H. et al. Right Ventricular Function After Pulmonary Artery Banding: Adaptive Processes Assessed by CMR and Conductance Catheter Measurements in Sheep. *Journal of Cardiovascular Translational Research*. **12** (5), 459–466 (2019).
35. Baicu, C. F. et al. Time course of right ventricular pressure-overload induced myocardial fibrosis: relationship to changes in fibroblast postsynthetic procollagen processing. *American Journal of Physiology-Heart and Circulatory Physiology*. **303** (9), H1128–H1134 (2012).
36. Manohar, M. et al. Regional myocardial blood flow and coronary vascular reserve in

unanesthetized young calves exposed to a simulated altitude of 3500 m for 8-10 weeks. *Circulation Research*. **50** (5), 714–726 (1982).
37. Fávaro, G. A. G. et al. Reversible pulmonary trunk banding: VII. Stress echocardiographic assessment of rapid ventricular hypertrophy in young goats. *Journal of Thoracic and Cardiovascular Surgery*. **145** (5) 1345–1351 (2013).
38. Nielsen, E. A. et al. Regional septal hinge-point injury contributes to adverse biventricular interactions in pulmonary hypertension. *Physiological Reports*. **5** (14), 1–13 (2017).
39. Borgdorff, M. A. et al. Sildenafil enhances systolic adaptation, but does not prevent diastolic dysfunction, in the pressure-loaded right ventricle. *European Journal of Heart Failure*. **14** (9), 1067–1074 (2012).
40. Gold, H., Prindle, K., Levey, G., Epstein, S. Effects of experimental heart failure on the capacity of glucagon to augment myocardial contractility and activate adenyl cyclase. *The Journal of Clinical Investigation*. **49** (5), 999–1006 (1970).
41. Brittain, E. L. et al. Right ventricular plasticity and functional imaging. *Pulmonary Circulation*. **2** (3), 309–326 (2012).
42. Jiang, L. et al. Three-dimensional Echocardiography In Vivo Validation for Right Ventricular Volume and Function. **89**, 2342–2350 (1994).
43. Markiewicz, W., Sechtem, U., Higgins, C. B. Evaluation of the right ventricle by magnetic resonance imaging. *American Heart Journal*. **113** (1), 8–15 (1987).
44. Pattynama, P. M. T. et al. Reproducibility of MRI-derived measurements of right ventricular volumes and myocardial mass. *Magnetic Resonance Imaging*. **13** (1), 53–63 (1995).
45. Wiesmann, F. et al. Comparison of fast spiral, echo planar, and fast low-angle shot MRI for cardiac volumetry at .5T. *Journal of Magnetic Resonance Imaging*. **8** (5), 1033–1039 (1998).
46. Van der Feen, D. E. et al. Multicenter Preclinical Validation of BET Inhibition for the Treatment of Pulmonary Arterial Hypertension. *American Journal of Respiratory and Critical Care Medicine*. **200** (7), 910–920 (2019).
47. da Costa Martins, P. A. et al. MicroRNA-199b targets the nuclear kinase Dyrk1a in an auto-amplification loop promoting calcineurin/NFAT signalling. *Nature Cell Biology*. **12** (12), 1220–1227 (2010).
48. Cheng, H.-W. et al. Assessment of right ventricular structure and function in mouse model of pulmonary artery constriction by transthoracic echocardiography. *Journal of Visualized Experiments*. (84), e51041 (2014).
49. Schulz-Menger, J. et al. Standardized image interpretation and post processing in cardiovascular magnetic resonance: Society for Cardiovascular Magnetic Resonance (SCMR) Board of Trustees Task Force on Standardized Post Processing. *Journal of Cardiovascular Magnetic Resonance*. **15** (1), 1–19 (2013).
50. Hagdorn, Q. A. J. et al. A novel method optimizing the normalization of cardiac parameters in small animal models: The importance of dimensional indexing. *American Journal of Physiology - Heart and Circulatory Physiology*. **316** (6), H1552–H1557 (2019).
51. Scherrer-Crosbie, M. et al. Determination of Right Ventricular Structure and Function in Normoxic and Hypoxic Mice. *Circulation*. **98** (10), 1015–1021 (2012).
52. Wiesmann, F. et al. Analysis of right ventricular function in healthy mice and a murine model of heart failure by in vivo MRI. *American Journal of Physiology-Heart and Circulatory Physiology*. **283** (3), H1065–H1071 (2002).

53. Lu, X. et al. Accuracy and Reproducibility of Real-Time Three-Dimensional Echocardiography for Assessment of Right Ventricular Volumes and Ejection Fraction in Children. *Journal of the American Society of Echocardiography*. **21** (1), 84–89 (2008).
54. Soriano, B. D. et al. Matrix-array 3-dimensional echocardiographic assessment of volumes, mass, and ejection fraction in young pediatric patients with a functional single ventricle: A comparison study with cardiac magnetic resonance. *Circulation*. **117** (14), 1842–1848 (2008).
55. Damy, T. et al. Prevalence of, associations with, and prognostic value of tricuspid annular plane systolic excursion (TAPSE) among out-patients referred for the evaluation of heart failure. *Journal of Cardiac Failure*. **18** (3), 216–225 (2012).
56. Kowalik, E., Kowalski, M., Rózański, J., Kuśmierczyk, M., Hoffman, P. The impact of pulmonary regurgitation on right ventricular regional myocardial function: An echocardiographic study in adults after total repair of tetralogy of fallot. *Journal of the American Society of Echocardiography*. **24** (11), 1199–1204 (2011).
57. Koestenberger, M. et al. Systolic right ventricular function in pediatric and adolescent patients with tetralogy of Fallot: Echocardiography versus magnetic resonance imaging. *Journal of the American Society of Echocardiography*. **24** (1), 45–52 (2011).
58. Bovens, S. M. et al. Evaluation of infarcted murine heart function: Comparison of prospectively triggered with self-gated MRI. *NMR in Biomedicine*. **24** (3), 307–315 (2011).

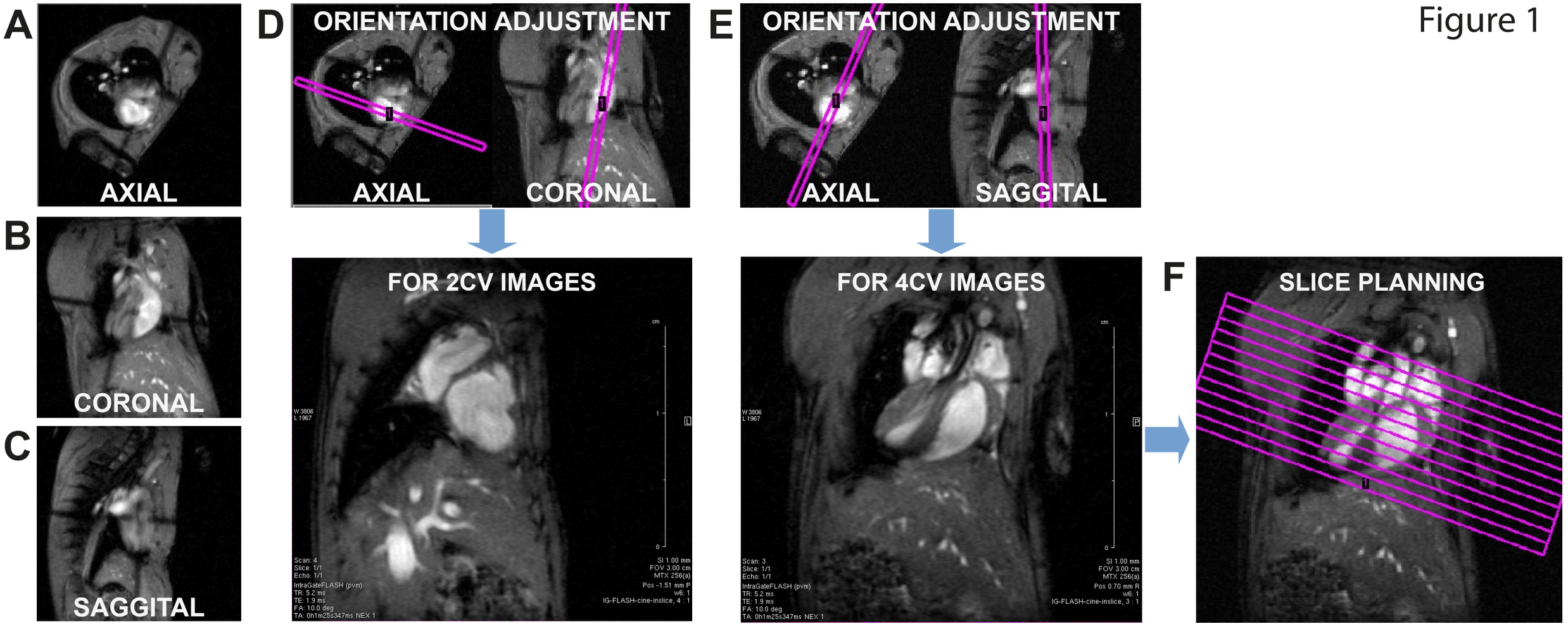

Figure 1

Figure 2

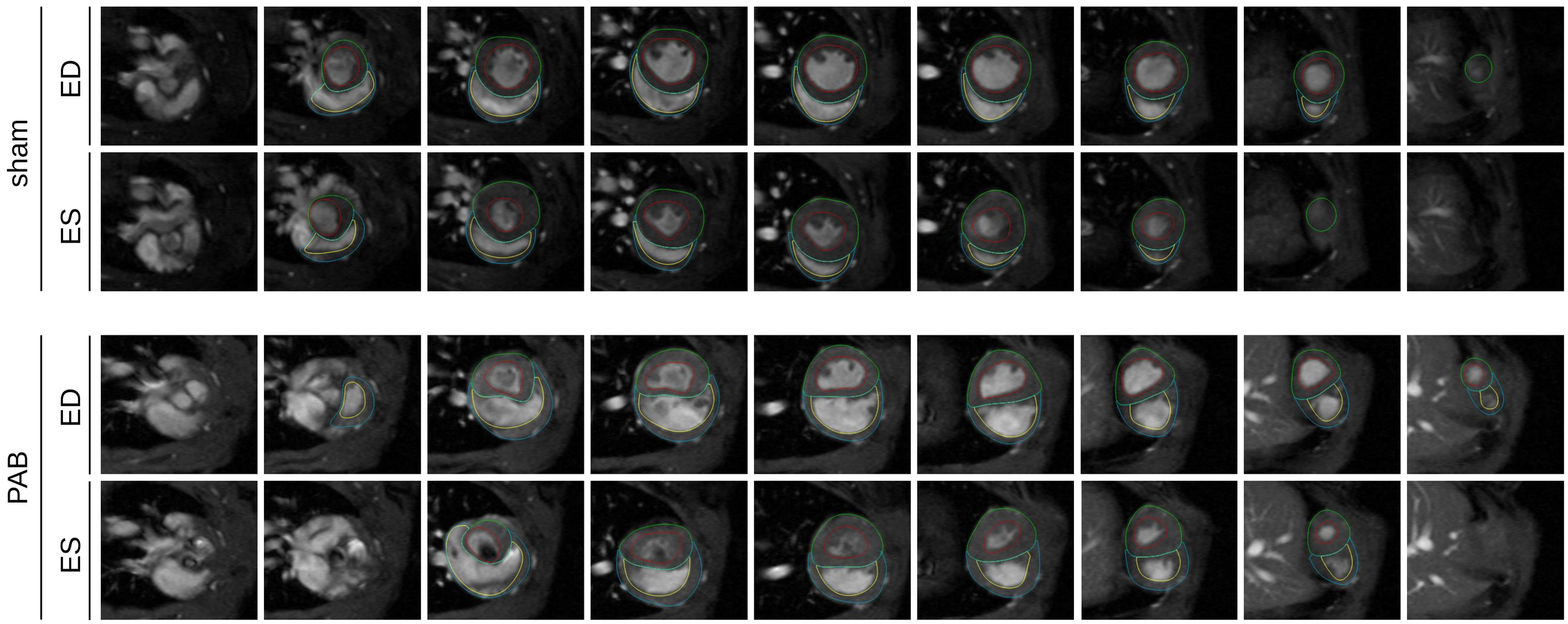

Figure 3

Figure 3

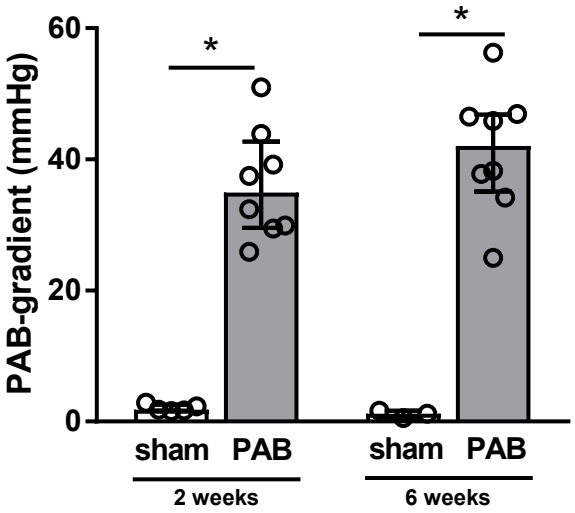

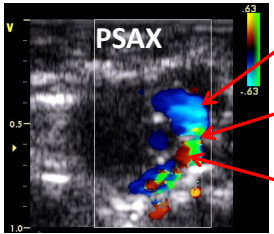

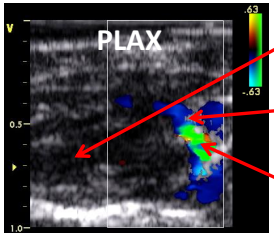

Figure 4

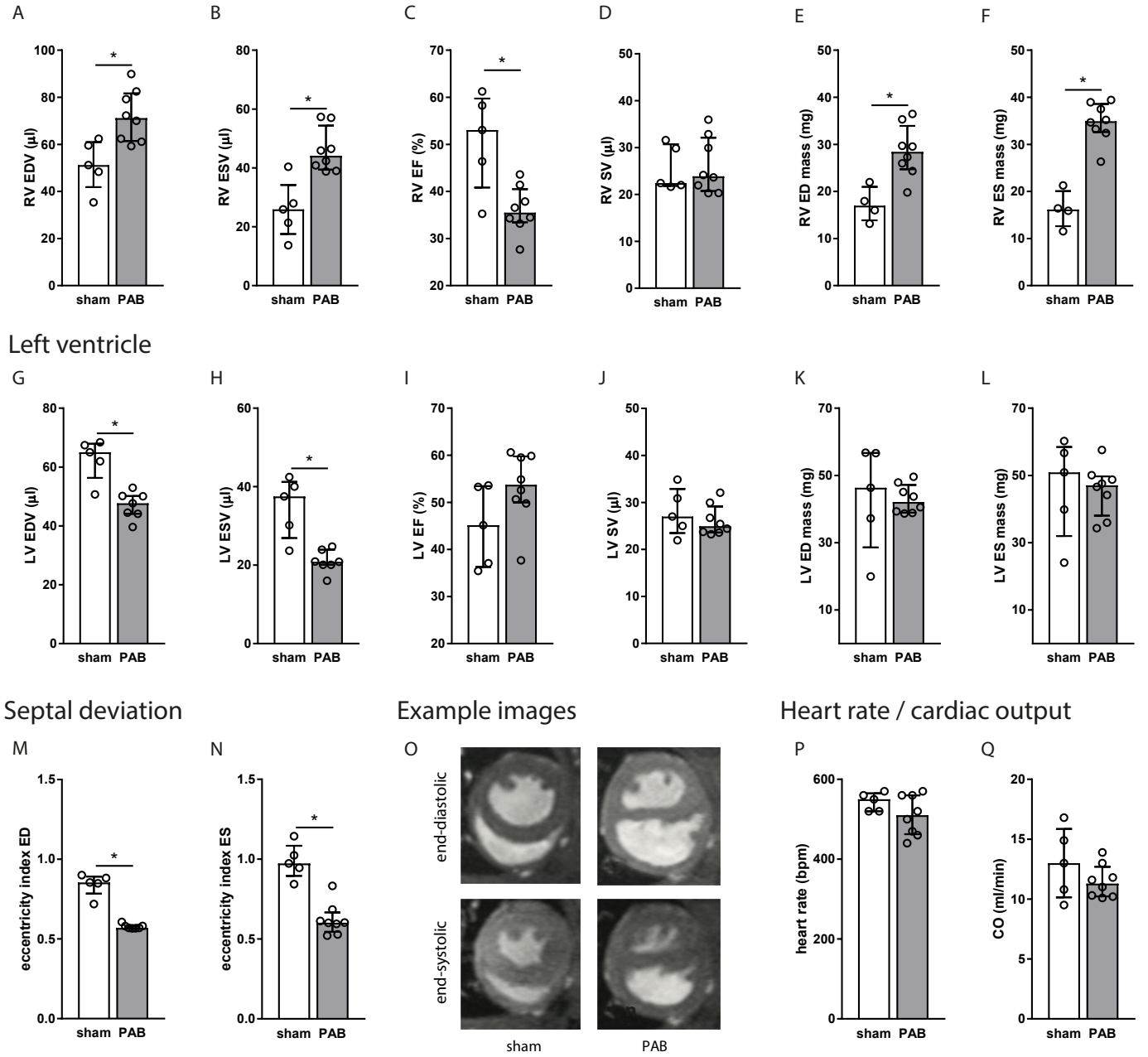

Table 1

Echo time (ms)	1.286
Repetition time (ms)	9.226
Radiofrequency pulse (ms)	0.300
Flip angle (degrees)	10
Spectral width (Hz)	75,757
Echo position (%)	20
Acquisition m atrix	256 x 128
Reconstructed matrix	256 x 256
In-plane resolution (µm)	117x117
Averages	8
Frames per heart beat	15
Slice thickness (mm)	1
Navigator points	256
Acquisition time per slice (s)	120

Name of Material/ Equipment	Company
14.0 MHz i13L-echocardiography transducer	GE Healthcare, Waukesha, WI, USA
20G cannula	
23G needle	
9.4T magnetic resonance scanner with 1,500 mT/m gradient set	Bruker BioSpin, Ellingen, Germany
Anesthesia induction chamber	
Blunt 25G needle	
Buprenorphine	
Chloride-hexidine	
CMR post-processing software	Medis Medical Imaging Systems, Leiden, The
Data visualisation and statistical software	GraphPad Prism Inc, La Jolla, CA, USA
Echocardiography machine	GE Healthcare, Waukesha, WI, USA
Eye ointment	
Heat mat	
Incubator (37°C)	
Isoflurane	
Isoflurane evaporator	
Miniventilator for rodents	Hugo Sachs
monofilament polypropylene 5-0 sutures	
monofilament polypropylene 6-0 sutures	
Needle and syringe for subcutaneous injections	
Pediatric electrocardiogram-stickers	
pure polyglycolic acid 5-0 sutures	
Sterile surgical instruments	
Ventilation mask	

Catalog Number	Comments/Description
Netherlands	Qmass version 7.6 software version 7.02 Vivid Dimension 7
model 687	

Rotterdam, 19-01-2020

Dear editor,

Hereby we resubmit our paper entitled “Quantification of Biventricular Function and Morphology by Cardiac Magnetic Resonance Imaging in Mice with Pulmonary Artery Banding”. We thank the editor and the reviewers for their careful comments and suggestions. With these suggestions, we have improved our manuscript. These points are now included in the revised manuscript as explained below. In addition, we have adjusted certain textual parts according to the suggestions of the reviewer. The responses to all the comments posed (in *italics*) are listed below point by point. The changes in the manuscript are in **bold**.

We believe the revised version meets the requirements for publication in the Journal of Visualized Experiments. If there are any additional questions, we will be glad to answer these.

Yours sincerely,

On behalf of the authors,

Anne-Marie Koop

Reviewers' comments

Reviewer #3:
Manuscript Summary:
The manuscript has been changed in some aspects in the resubmitted form. However, some points mentioned initially have not been addressed.

Major Concerns:
1. The paper describes two approaches of the MR imaging: self-gated and prospective EGC triggered FLASH. For a reader, being not from the field, it would be helpful to have a short introduction into these two approaches with discussion of their advantages and limitations.

We thank the reviewer for his or her comment. We agree that the first version of the manuscript may have been insufficiently clear regarding the triggering of the CMR. Based on the suggestion of the reviewer and In order to generate a protocol which is as explicate as possible, we decided to only describe the one method we use in our institution, and which is currently considered as the golden standard. In the discussion we explain our considerations.

The current protocol describes the use of self-gated CMR, which obviates the need for ECG triggering and respiratory gating. This method has been described previously in a report from the same institution, demonstrating good intra- and inter-observer variability. (Bovens et al., 2011) **Another method that could be used if the self-gated method were to be unavailable, is prospective ECG triggering. However, in a previous report from our institution, it was demonstrated that the self-gated method provides less variability, better signal and contrast to noise ratios, and less arrhythmia induced artifacts. Therefore, we recommend using the self-gated method, as stated in the current protocol.** (Line 502-509)

2. Please provide a table comparing results obtained by the two methods including comparison statistics and variability.

Indeed, validation of used techniques is desirable. As discussed above, intra- and inter observer variability of self-gated CMR in the murine heart have been previously studied in our institution and reported by Bovens, et al. The results demonstrate good inter- and intra-observer variability, and imply no differences in inter-observer variability in both healthy and diseased mice for both LV and RV volumes. Furthermore, it was demonstrated that the self-gated method provides less variability, better signal and contrast to noise ratios, and less arrhythmia induced artifacts. In addition, intra-observer variability regarding RV parameters improved by a short navigator. Since the self-gated method is more appropriate to prospectively triggered method, the self-gated method is preferred due its great advantage in time efficiency.

*Bovens, S.M. et al. Evaluation of infarcted murine heart function: Comparison of prospectively triggered with self-gated MRI. NMR in Biomedicine. **24** (3), 307–315, doi: 10.1002/nbm.1593 (2011).*

Reviewer #4:
Manuscript Summary:
It was a pleasure to review the paper "Quantification of Biventricular Function and Morphology by Cardiac Magnetic Resonance Imaging in Mice with Pulmonary Artery Banding". The authors present a pulmonary banding model and evaluation of RV anatomy and function using self-gating MR. The topic is relevant but the methods need some refinement before publishing: Precision on the PAB model is inadequate. Phase contrast should be included in the MR protocol. Intra-/inter operator-/observer data should be presented for the methods.

Comments:
1) Introduction is too long. Please shorten and focus the introduction to be precise and relevant for the topic you address.

Following the suggestion of the reviewer we have shortened the introduction.

2) I appreciate that you use the pressure gradient to ensure that the banding is precise, but I have 2 comments:

a. The gradient is affected by stroke volume. For a fixed stenosis you will get a high gradient with a high SV and a low gradient with a low SV. If you place a tight band that induces RV failure, SV will drop and you will get a low gradient despite a tight clip (Low Flow-Low Gradient phenomenon). This is a bias and should at least be mentioned.

We thank the reviewer for this comment. Indeed, stroke volume / cardiac output may affect the gradient across the pulmonary artery banding. However, this is the case in heart failure with reduced cardiac output. It therefore is important to perform the echocardiographic validation of the pulmonary artery banding gradient before cardiac output is affected. We performed the measurements after two weeks of increased RV loading, when cardiac output is still preserved. When heart failure with reduced cardiac output develops, the reciprocal relation of SV and the gradient arises and may complicate interpretation of these parameters. We have now addressed this mechanism in the discussion.

However, at termination, RV pressure is not only dependent of the "tightness" of the banding but becomes increasingly dependent of RV function. Whenever RV failure occurs within the duration of PAB, expressed by decreased cardiac output, and also RV systolic pressure will decrease, biasing results. Such biases can be avoided or minimized by assessing RV pressure load at 2 weeks after PAB surgery, instead of at termination. By means of echocardiography, assessment of RV afterload at this time point can be performed reliably and safely. This allows grouping of the mice into groups with equal pressure load, which could be helpful for intervention studies. Also, repeated measurements are easily feasible. *(Line 565-572)*

b. In figure 3 you present your PAB gradients and they are not very precise. You have gradients ranging from 25 - 55 mmHg. This is more than 100% increase from the lowest to the highest gradient. This is also reflected (I guess) in the very varying RV EF and RV SV you present in figure 4. RV EF range from 25-45% and RV SV range from 20-40 ul. With a model this imprecise it is very difficult to measure an effect of an intervention unless you include very high numbers. You need to improve the precision of the model.

The differences in gradients may reflect the tightness of the banding in different animals. Even though some variation in the degree of RV-pressure load remains inevitable, all obtained gradients represent a substantial and significant increase in RV pressure load and eventually lead to RV remodeling and adaptation of RV-function. Our ample experience with this model contributes to our strong opinion that our standardized surgical procedures result in a model of fixed and effective RV pressure load that is stable and reproducible

3) I would strongly suggest to include the use of phase contrast to measure SV which is considered gold standard. By using volumetry a tricuspid regurgitation will introduce a bias. Also the delineation of the RV in the tricuspid plane may be difficult to assess when using 1 mm slices in a mouse heart.

Despite the cited advantages of Phase Contrast technique, this PC method is sensitive to phase errors not related to myocardial motion. The main source for phase errors in our setup are eddycurrents, since our gradient system (1500mT/m) is not actively shielded. We were therefore not able to use Phase Contrast imaging.

4) When describing a method for evaluating RV function you need to include intra-/inter-operator-observer variations. How precise and accurate are the methods you present?

Inter- and intra-observer variability analyses have been performed and published by our group previously. In the current manuscript, we refer to this report (see below). In addition to the response at the comments of reviewer #3, Bovens, et al. reported the means and standard deviations of self-gated data, and comparison to prospectively-triggered data.

*Bovens, S.M. et al. Evaluation of infarcted murine heart function: Comparison of prospectively triggered with self-gated MRI. NMR in Biomedicine. **24** (3), 307–315, doi: 10.1002/nbm.1593 (2011).*

The current protocol describes the use of self-gated CMR, which obviates the need for ECG triggering and respiratory gating. This method has been described previously in a report from the same institution, demonstrating good intra- and inter-observer variability.[58] *(Line 552-552)*

Minor Concerns:
- fig 4 J/D: ul instead of ml

We thank the reviewer for his/her notice and corrected the figure accordingly.

Reviewer #5:
Manuscript Summary:
Very well written manuscript with a detailed and comprehensible model description, paying due attention to benefits and limitations of various experimental models of RV failure and methods for evaluation. I have only a few minor comments

Minor Concerns:
Could the authors provide a picture/diagram of the pulmonary artery banding with the 23G needle, which would improve the reproducibility for other researchers.

We thank the reviewer for his or her suggestions. We agree that visualization of the experiment would be of great added value. We therefor choose to include this part of the protocol in the video.

The number of animals included in the presented result section should be available, in order to let others get an impression of statistical power of the mouse model.

The reviewer suggested to incorporate the animal numbers in the result section. In the first revision we have already added the numbers in general. We have now added a supplementary table with the number per CMR parameter.

Supplementary table 1. Number of animals per hemodynamic parameter.

	sham	***PAB***
RV EDV	5	8
RV ESV	5	8
RV EF	5	8
RV SV	5	8
RV ED mass	4	8
RV ES mass	4	8
LV EDV	5	7
LV ESV	5	7
LV EF	5	8
LV SV	5	8
LV ED mass	5	8
LV ES mass	5	8
EI ED	5	7
EI ES	5	8
HR	5	8
CO	5	8

RV = right ventricle, EDV = end diastolic volume, ESV = end systolic volume, EF = ejection fraction, SV = stroke volume, ED mass = end diastolic mass, ES mass = end systolic mass, LV = left ventricle, EI ES = eccentricity index end systolic, EI ED = eccentricity index end diastolic, HR = heart rate, CO = cardiac output

If possible it would be interesting if the authors could provide coefficient of variation (CV,%), when analyzing CMR images, both within and between animals. Not necessarily for all images, but for instance a main end-point like RV-EDV.

We thank the reviewer for his suggestion. We have added a supplementary table with the coefficient of variation for each parameter included in figure 4.

Supplementary table 2. Coefficient of variation per hemodynamic parameter.

	sham	***PAB***
RV EDV	20,7	15,4
RV ESV	37,9	16,3
RV EF	20,4	13,8
RV SV	18,8	23,0
RV ED mass	21,5	19,3
RV ES mass	24,4	12,2
LV EDV	11,4	9,7
LV ESV	22,2	13,6
LV EF	19,2	14,2
LV SV	18,0	12,5
LV ED mass	35,5	10,0
LV ES mass	31,6	16,6
EI ED	8,5	2,4
EI ES	11,1	15,9
HR	4,2	9,9
CO	22,8	12,1

RV = right ventricle, EDV = end diastolic volume, ESV = end systolic volume, EF = ejection fraction, SV = stroke volume, ED mass = end diastolic mass, ES mass = end systolic mass, LV = left ventricle, EI ES = eccentricity index end systolic, EI ED = eccentricity index end diastolic, HR = heart rate, CO = cardiac output

Reviewer #6:

Manuscript Summary:

In the current manuscript Koop and co-authors presented protocol for the quantitative analyses of the cardiac function and morphology in comprehensive animal model of right ventricular pressure overload. The authors presented very detailed protocol for pressure gradient measurement by echocardiography and right and left ventricular function/mass by cardiac MRI. The manuscript is well

written and presented in a very adequate way.

Minor Concerns:
1) As I have recognized the echocardiographic measurements were performed with Vivi7. It would be great if authors will add the model of transducer and its frequency to the protocol.

As suggested by the reviewer, we have now added the frequency of the transducer in the protocol. Indeed echocardiographic measurements were performed by a Vivid Dimension 7 with a i13L-transducer, with a 5.8 to 14.0 MHz frequency range *(GE Healthcare, Waukesha, WI, USA), to our knowledge we are not allowed to mention this in the protocol. We do now have this information incorporated in the Table of Materials.*

2) The analyses of the common indexes of the RV function as a longitudinal and transverse shortening were performed by several authors by using cardiac MRI (e.g. Kind et al., 2010, Swift et al., 2015). It would be nice if authors will discuss in the manuscript the fSFD and fTAAD measurements as well.

We thank the reviewer for his or her suggestion. The expansion of parameters of right ventricular function in specific directions (longitudinal vs. transverse shortening) may provide additional insight into patterns of functional RV adaptation. Fractional septum to free wall distance at the mid of the RV (fSFD) and fractional tricuspid annulus-apex distance change (fTAAD) are related to both transverse motion and RV ejection fraction compared to longitudinal motion.(Kojonazarov et al., 2018) *In addition, transverse motion at mid RV is significantly stronger associated with RVEF compared to longitudinal motion. Hereby, transverse motion may be a better predictor of RV function. In the current study, we have focused on parameters as used in clinical CMR. In our CMR research protocol in mice the suggested (non-volume based) functional RV parameters are not incorporated. Therefore, we could not add the reviewers #6 suggested measurements. However, readers and researchers, with interest in these measurements can of course incorporate these in their respective protocols.*

Kojonazarov, B. et al. Evaluating Systolic and Diastolic Cardiac Function in Rodents Using Microscopic Computed Tomography. Circulation: Cardiovascular Imaging. 2018;11:e007653. DOI: 10.1161/CIRCIMAGING.118.007653.

Supplementary table 1. Number of animals per hemodynamic parameter.

	sham	***PAB***
RV EDV	5	8
RV ESV	5	8
RV EF	5	8
RV SV	5	8
RV ED mass	4	8
RV ES mass	4	8
LV EDV	5	7
LV ESV	5	7
LV EF	5	8
LV SV	5	8
LV ED mass	5	8
LV ES mass	5	8
EI ED	5	7
EI ES	5	8
HR	5	8
CO	5	8

RV = right ventricle, EDV = end diastolic volume, ESV = end systolic volume, EF = ejection fraction, SV = stroke volume, ED mass = end diastolic mass, ES mass = end systolic mass, LV = left ventricle, EI ES = eccentricity index end systolic, EI ED = eccentricity index end diastolic, HR = heart rate, CO = cardiac output

Supplementary table 2. Coefficient of variation per hemodynamic parameter.

	sham	***PAB***
RV EDV	20,7	15,4
RV ESV	37,9	16,3
RV EF	20,4	13,8
RV SV	18,8	23,0
RV ED mass	21,5	19,3
RV ES mass	24,4	12,2
LV EDV	11,4	9,7
LV ESV	22,2	13,6
LV EF	19,2	14,2
LV SV	18,0	12,5
LV ED mass	35,5	10,0
LV ES mass	31,6	16,6
EI ED	8,5	2,4
EI ES	11,1	15,9
HR	4,2	9,9
CO	22,8	12,1

RV = right ventricle, EDV = end diastolic volume, ESV = end systolic volume, EF = ejection fraction, SV = stroke volume, ED mass = end diastolic mass, ES mass = end systolic mass, LV = left ventricle, EI ES = eccentricity index end systolic, EI ED = eccentricity index end diastolic, HR = heart rate, CO = cardiac output

jove JOURNAL OF VISUALIZED EXPERIMENTS
1 Alewife Center #200
Cambridge, MA 02140
tel. 617.945.9051
www.jove.com

ARTICLE AND VIDEO LICENSE AGREEMENT

Title of Article:	Quantification of Biventricular Function and Morphology by Cardiac Magnetic Resonance Imaging in Mice with Pulmonary Artery Banding
Author(s):	A.M.C. Koop , et al.

Item 1: The Author elects to have the Materials be made available (as described at http://www.jove.com/publish) via:

☑ Standard Access ☐ Open Access

Item 2: Please select one of the following items:

☑ The Author is **NOT** a United States government employee.

☐ The Author is a United States government employee and the Materials were prepared in the course of his or her duties as a United States government employee.

☐ The Author is a United States government employee but the Materials were NOT prepared in the course of his or her duties as a United States government employee.

ARTICLE AND VIDEO LICENSE AGREEMENT

1. **Defined Terms.** As used in this Article and Video License Agreement, the following terms shall have the following meanings: "**Agreement**" means this Article and Video License Agreement; "**Article**" means the article specified on the last page of this Agreement, including any associated materials such as texts, figures, tables, artwork, abstracts, or summaries contained therein; "**Author**" means the author who is a signatory to this Agreement; "**Collective Work**" means a work, such as a periodical issue, anthology or encyclopedia, in which the Materials in their entirety in unmodified form, along with a number of other contributions, constituting separate and independent works in themselves, are assembled into a collective whole; "**CRC License**" means the Creative Commons Attribution-Non Commercial-No Derivs 3.0 Unported Agreement, the terms and conditions of which can be found at: http://creativecommons.org/licenses/by-nc-nd/3.0/legalcode; "**Derivative Work**" means a work based upon the Materials or upon the Materials and other pre-existing works, such as a translation, musical arrangement, dramatization, fictionalization, motion picture version, sound recording, art reproduction, abridgment, condensation, or any other form in which the Materials may be recast, transformed, or adapted; "**Institution**" means the institution, listed on the last page of this Agreement, by which the Author was employed at the time of the creation of the Materials; "**JoVE**" means MyJove Corporation, a Massachusetts corporation and the publisher of The Journal of Visualized Experiments; "**Materials**" means the Article and / or the Video; "**Parties**" means the Author and JoVE; "**Video**" means any video(s) made by the Author, alone or in conjunction with any other parties, or by JoVE or its affiliates or agents, individually or in collaboration with the Author or any other parties, incorporating all or any portion of the Article, and in which the Author may or may not appear.

2. **Background.** The Author, who is the author of the Article, in order to ensure the dissemination and protection of the Article, desires to have the JoVE publish the Article and create and transmit videos based on the Article. In furtherance of such goals, the Parties desire to memorialize in this Agreement the respective rights of each Party in and to the Article and the Video.

3. **Grant of Rights in Article.** In consideration of JoVE agreeing to publish the Article, the Author hereby grants to JoVE, subject to **Sections 4** and **7** below, the exclusive, royalty-free, perpetual (for the full term of copyright in the Article, including any extensions thereto) license (a) to publish, reproduce, distribute, display and store the Article in all forms, formats and media whether now known or hereafter developed (including without limitation in print, digital and electronic form) throughout the world, (b) to translate the Article into other languages, create adaptations, summaries or extracts of the Article or other Derivative Works (including, without limitation, the Video) or Collective Works based on all or any portion of the Article and exercise all of the rights set forth in (a) above in such translations, adaptations, summaries, extracts, Derivative Works or Collective Works and(c) to license others to do any or all of the above. The foregoing rights may be exercised in all media and formats, whether now known or hereafter devised, and include the right to make such modifications as are technically necessary to exercise the rights in other media and formats. If the "Open Access" box has been checked in **Item 1** above, JoVE and the Author hereby grant to the public all such rights in the Article as provided in, but subject to all limitations and requirements set forth in, the CRC License.

4. **Retention of Rights in Article.** Notwithstanding the exclusive license granted to JoVE in **Section 3** above, the Author shall, with respect to the Article, retain the non-exclusive right to use all or part of the Article for the non-commercial purpose of giving lectures, presentations or teaching classes, and to post a copy of the Article on the Institution's website or the Author's personal website, in each case provided that a link to the Article on the JoVE website is provided and notice of JoVE's copyright in the Article is included. All non-copyright intellectual property rights in and to the Article, such as patent rights, shall remain with the Author.

5. **Grant of Rights in Video – Standard Access.** This **Section 5** applies if the "Standard Access" box has been checked in **Item 1** above or if no box has been checked in **Item 1** above. In consideration of JoVE agreeing to produce, display or otherwise assist with the Video, the Author hereby acknowledges and agrees that, Subject to **Section 7** below, JoVE is and shall be the sole and exclusive owner of all rights of any nature, including, without limitation, all copyrights, in and to the Video. To the extent that, by law, the Author is deemed, now or at any time in the future, to have any rights of any nature in or to the Video, the Author hereby disclaims all such rights and transfers all such rights to JoVE.

6. **Grant of Rights in Video – Open Access.** This **Section 6** applies only if the "Open Access" box has been checked in **Item 1** above. In consideration of JoVE agreeing to produce, display or otherwise assist with the Video, the Author hereby grants to JoVE, subject to **Section 7** below, the exclusive, royalty-free, perpetual (for the full term of copyright in the Article, including any extensions thereto) license (a) to publish, reproduce, distribute, display and store the Video in all forms, formats and media whether now known or hereafter developed (including without limitation in print, digital and electronic form) throughout the world, (b) to translate the Video into other languages, create adaptations, summaries or extracts of the Video or other Derivative Works or Collective Works based on all or any portion of the Video and exercise all of the rights set forth in (a) above in such translations, adaptations, summaries, extracts, Derivative Works or Collective Works and (c) to license others to do any or all of the above. The foregoing rights may be exercised in all media and formats, whether now known or hereafter devised, and include the right to make such modifications as are technically necessary to exercise the rights in other media and formats. For any Video to which this **Section 6** is applicable, JoVE and the Author hereby grant to the public all such rights in the Video as provided in, but subject to all limitations and requirements set forth in, the CRC License.

7. **Government Employees.** If the Author is a United States government employee and the Article was prepared in the course of his or her duties as a United States government employee, as indicated in **Item 2** above, and any of the licenses or grants granted by the Author hereunder exceed the scope of the 17 U.S.C. 403, then the rights granted hereunder shall be limited to the maximum rights permitted under such statute. In such case, all provisions contained herein that are not in conflict with such statute shall remain in full force and effect, and all provisions contained herein that do so conflict shall be deemed to be amended so as to provide to JoVE the maximum rights permissible within such statute.

8. **Protection of the Work.** The Author(s) authorize JoVE to take steps in the Author(s) name and on their behalf if JoVE believes some third party could be infringing or might infringe the copyright of either the Author's Article and/or Video.

9. **Likeness, Privacy, Personality.** The Author hereby grants JoVE the right to use the Author's name, voice, likeness, picture, photograph, image, biography and performance in any way, commercial or otherwise, in connection with the Materials and the sale, promotion and distribution thereof. The Author hereby waives any and all rights he or she may have, relating to his or her appearance in the Video or otherwise relating to the Materials, under all applicable privacy, likeness, personality or similar laws.

10. **Author Warranties.** The Author represents and warrants that the Article is original, that it has not been published, that the copyright interest is owned by the Author (or, if more than one author is listed at the beginning of this Agreement, by such authors collectively) and has not been assigned, licensed, or otherwise transferred to any other party. The Author represents and warrants that the author(s) listed at the top of this Agreement are the only authors of the Materials. If more than one author is listed at the top of this Agreement and if any such author has not entered into a separate Article and Video License Agreement with JoVE relating to the Materials, the Author represents and warrants that the Author has been authorized by each of the other such authors to execute this Agreement on his or her behalf and to bind him or her with respect to the terms of this Agreement as if each of them had been a party hereto as an Author. The Author warrants that the use, reproduction, distribution, public or private performance or display, and/or modification of all or any portion of the Materials does not and will not violate, infringe and/or misappropriate the patent, trademark, intellectual property or other rights of any third party. The Author represents and warrants that it has and will continue to comply with all government, institutional and other regulations, including, without limitation all institutional, laboratory, hospital, ethical, human and animal treatment, privacy, and all other rules, regulations, laws, procedures or guidelines, applicable to the Materials, and that all research involving human and animal subjects has been approved by the Author's relevant institutional review board.

11. **JoVE Discretion.** If the Author requests the assistance of JoVE in producing the Video in the Author's facility, the Author shall ensure that the presence of JoVE employees, agents or independent contractors is in accordance with the relevant regulations of the Author's institution. If more than one author is listed at the beginning of this Agreement, JoVE may, in its sole

discretion, elect not take any action with respect to the Article until such time as it has received complete, executed Article and Video License Agreements from each such author. JoVE reserves the right, in its absolute and sole discretion and without giving any reason therefore, to accept or decline any work submitted to JoVE. JoVE and its employees, agents and independent contractors shall have full, unfettered access to the facilities of the Author or of the Author's institution as necessary to make the Video, whether actually published or not. JoVE has sole discretion as to the method of making and publishing the Materials, including, without limitation, to all decisions regarding editing, lighting, filming, timing of publication, if any, length, quality, content and the like.

12. **Indemnification.** The Author agrees to indemnify JoVE and/or its successors and assigns from and against any and all claims, costs, and expenses, including attorney's fees, arising out of any breach of any warranty or other representations contained herein. The Author further agrees to indemnify and hold harmless JoVE from and against any and all claims, costs, and expenses, including attorney's fees, resulting from the breach by the Author of any representation or warranty contained herein or from allegations or instances of violation of intellectual property rights, damage to the Author's or the Author's institution's facilities, fraud, libel, defamation, research, equipment, experiments, property damage, personal injury, violations of institutional, laboratory, hospital, ethical, human and animal treatment, privacy or other rules, regulations, laws, procedures or guidelines, liabilities and other losses or damages related in any way to the submission of work to JoVE, making of videos by JoVE, or publication in JoVE or elsewhere by JoVE. The Author shall be responsible for, and shall hold JoVE harmless from, damages caused by lack of sterilization, lack of cleanliness or by contamination due to the making of a video by JoVE its employees, agents or independent contractors. All sterilization, cleanliness or decontamination procedures shall be solely the responsibility of the Author and shall be undertaken at the Author's expense. All indemnifications provided herein shall include JoVE's attorney's fees and costs related to said losses or damages. Such indemnification and holding harmless shall include such losses or damages incurred by, or in connection with, acts or omissions of JoVE, its employees, agents or independent contractors.

13. **Fees.** To cover the cost incurred for publication, JoVE must receive payment before production and publication of the Materials. Payment is due in 21 days of invoice. Should the Materials not be published due to an editorial or production decision, these funds will be returned to the Author. Withdrawal by the Author of any submitted Materials after final peer review approval will result in a US$1,200 fee to cover pre-production expenses incurred by JoVE. If payment is not received by the completion of filming, production and publication of the Materials will be suspended until payment is received.

14. **Transfer, Governing Law.** This Agreement may be assigned by JoVE and shall inure to the benefits of any of JoVE's successors and assignees. This Agreement shall be governed and construed by the internal laws of the Commonwealth of Massachusetts without giving effect to any conflict of law provision thereunder. This Agreement may be executed in counterparts, each of which shall be deemed an original, but all of which together shall be deemed to me one and the same agreement. A signed copy of this Agreement delivered by facsimile, e-mail or other means of electronic transmission shall be deemed to have the same legal effect as delivery of an original signed copy of this Agreement.

A signed copy of this document must be sent with all new submissions. Only one Agreement is required per submission.

CORRESPONDING AUTHOR

Name:	Anne-Marie Catherine Koop
Department:	Department of Pediatric Cardiology
Institution:	Univerisity Medical Center Groningen
Title:	MD

Signature: AMCK Date: 10/04/2019

Please submit a **signed** and **dated** copy of this license by one of the following three methods:

1. Upload an electronic version on the JoVE submission site
2. Fax the document to +1.866.381.2236
3. Mail the document to JoVE / Attn: JoVE Editorial / 1 Alewife Center #200 / Cambridge, MA 02140

Signature Certificate

Document Ref.: NHVUA-5K795-AFEKZ-XAOVM

Document signed by:

Anne-Marie Koop

Verified E-mail:
a.c.koop@umcg.nl

AMCK

IP: 192.87.23.66 Date: 05 Oct 2019 05:59:18 UTC

Document completed by all parties on:
05 Oct 2019 05:59:18 UTC